

Hydrogen Addition for Centimeter-sized Monolayer Tungsten Disulfide Continuous Films by Ambient Pressure Chemical Vapor Deposition

Yuewen Sheng¹, Haijie Tan¹, Xiaochen Wang¹, Jamie H. Warner^{1}*

¹Department of Materials, University of Oxford, Parks Road, Oxford, OX1 3PH, United Kingdom

ABSTRACT

Monolayer tungsten disulfide (WS₂) offers great prospects for use in optoelectronic devices due to its direct bandgap and high photoluminescence intensity. Here, we show how the controlled addition of hydrogen into the chemical vapor deposition growth of WS₂ can lead to the formation of centimeter scale continuous monolayer films at ambient pressure without the need for seed molecules, specially prepared substrates or low pressure vacuum systems. Modifications of the reaction conditions, including growth time and hydrogen to argon ratio, allow for control over the domain size, film coverage and film uniformity of the prepared WS₂ film. The combined control of hydrogen and a double-furnace system enables an increase in the growth rate of WS₂, resulting in fully-merged films with cm² coverage and reduced multilayer content. Field effect transistors are fabricated to demonstrate the WS₂ has high quality for electronic applications. Our APCVD reaction is simple and efficient, ideal for mass-production of large area monolayer WS₂.

INTRODUCTION

The monolayer transition metal dichalcogenides (TMDs) with the formula MX_2 ($\text{M}=\text{W}, \text{Mo}$; $\text{X}=\text{S}, \text{Se}$) consists of a metal layer (Mo, W , etc.) sandwiched by two planes of chalcogen atoms (S, Se or Te).¹ Unlike semi-metallic graphene²⁻⁷ and insulating hexagonal boron nitride,⁸⁻¹¹ atomically thin two-dimensional (2D) TMDs are semiconductors bonded to neighboring layers via weak van der Waals force with desirable direct band gaps transitioning from 1 to 2 eV when their thickness is reduced from bulk to a single layer. This makes monolayer TMDs promising for applications in electronics, optoelectronics and valleytronics.¹²⁻²¹

As two typical members of the TMD family, tungsten disulfide (WS_2) and molybdenum disulfide (MoS_2) have been the focus of many studies in recent years.²²⁻²⁴ Many methods have been explored to prepare ultrathin WS_2 , including mechanical exfoliation,²⁵⁻²⁷ chemically assisted exfoliation²⁸, pulsed laser deposition¹³ and chemical vapor deposition (CVD).^{29,30} The top-down exfoliation methods can normally produce high quality crystals but only allow limited control over domain size, shape and coverage. The deposition of large area WS_2 films is essential for further application research and commercialization. Therefore, the bottom-up growth of WS_2 samples via the CVD approach has drawn great attention and has become the most cost effective and reliable mean to produce large-area high quality WS_2 thin films.²⁹⁻³⁴

Prior work has shown that large-area WS_2 sheets from single to few-layer thickness can be formed on silicon wafers which have a surface oxide layer (SiO_2/Si) by thermal reduction-sulfurization method,³⁰ and a wavelength sensitive photodetector can be fabricated based on the few-layer WS_2 films grown by the same method using a quartz substrate.³⁴ Hussain et al.³¹ presented a similar preparation technique via sulfurization of a RF-sputtered tungsten oxide (WO_3) film to produce continuous and wafer-scale uniform WS_2 layers. The photoresponse was also investigated in the

report based on few-layer samples, indicating that the photosensitivity was linearly dependent on bias voltage.³¹ Kang et al.³² achieved polycrystalline WS₂ monolayer up to mm² using two stacked substrates facing each other, one for the tungsten source and the other for growth. They also studied the effect of hydrogen (H₂) concentration on the growth results, including crystal size, nucleation density and growth formation.³² These methods described above seem to be appropriate for growing large-area continuous WS₂ films. However, the grain size of the film is mostly limited to nanoscale, which will result in poor device performance. In addition, all the reactions were carried out under vacuum or low pressure with a growth duration of ~30 minutes, hindering the viability of these processes for mass-production of WS₂. To increase grain size, shorten the growth time, and alleviate the difficulty of CVD setup, perylene-3,4,9,10-tetracarboxylic acid tetrapotassium salt (PTAS) has been introduced to grow large-area (~mm²) monolayer WS₂ films in 10 minutes by ambient pressure chemical vapor deposition (APCVD).^{33,35} However, the seeding promotor may produce impurities on the surface, and it is challenging to achieve full coverage without multilayer regions. Another approach demonstrated by Yun et al.¹² is to use an Au substrate instead of an insulating substrate. It is reported that centimeter-sized WS₂ film can be grown on Au in 15 minutes via APCVD, however, special treatment is required for preparing Au substrates and the compulsory transfer of the film after growth may generate cracks, which will slow and hinder device fabrication.^{12,36}

In this work, we demonstrate how hydrogen addition can be used to improve growth conditions within APCVD to achieve monolayer WS₂ continuous films exhibiting cm² coverage, grown on insulating substrates (SiO₂/Si) using separately-introduced solid powder precursors (S and WO₃) by APCVD. By using a two-furnace system, we are able to separately control the S and WO₃ precursor introduction and fine tune reaction parameters with incorporated H₂ gas flow to realize

uniform thin monolayer films. The quality and uniformity of the fully covered continuous films were then characterized by optical microscopy, scanning electron microscopy (SEM), atomic force microscopy (AFM), photoluminescence (PL) spectroscopy and Raman spectroscopy. Furthermore, we demonstrated the fabrication and performance of a WS₂ field effect transistor (FET).

RESULTS AND DISCUSSION

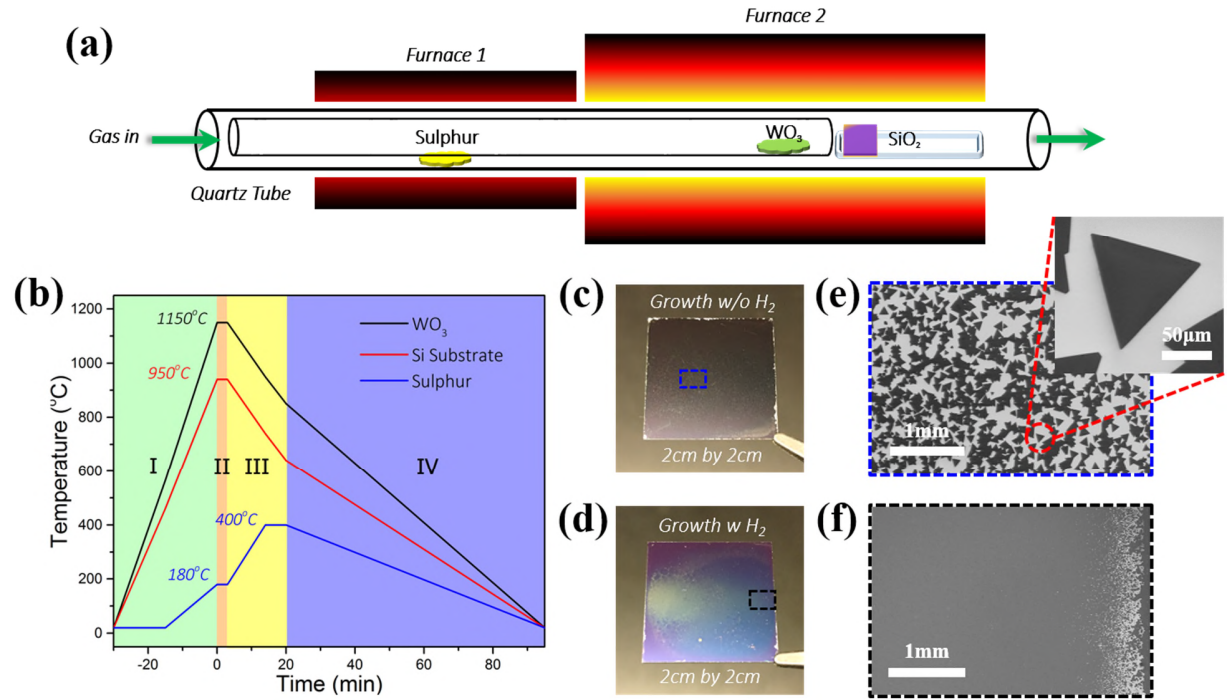


Figure 1. Atmospheric pressure CVD synthesis of large-area WS_2 films and domains on the SiO_2/Si substrate. (a) Schematic illustration of the CVD setup for the synthesis of WS_2 . Sulfur (S) and WO_3 powder were placed in a 1 inch quartz tube running through two furnace systems to provide two heating zones. (b) Temperature profiles of the substrate, WO_3 and S. The growth can be divided into four steps, including (I) heating stage, (II) growth stage, (III) slow cooling and sulfur purging, followed by (IV) fast cooling. (c, d) Photos showing contrast difference between 2 cm by 2 cm SiO_2/Si substrates after CVD processes without and with H_2 addition. (e) SEM image of large triangular WS_2 crystals deposited on a SiO_2/Si substrate. Scale bar: 1 mm. The zoomed-in SEM image indicates that the size of a typical crystal is around $150\text{ }\mu\text{m}$. Inset scale bar: $50\text{ }\mu\text{m}$. (f) SEM image of a millimeter-sized WS_2 film on SiO_2/Si . Scale bar: 1 mm.

Figure 1(a) shows a schematic illustration of our standard experimental setup for growing our monolayer WS_2 samples.³⁷⁻³⁹ The growth was conducted within a 1 inch diameter quartz tube under ambient pressure with a mixed flow of H_2 and Ar. Sulfur powders was loaded at the center

of low temperature furnace (furnace 1) in the outer 1 inch quartz tube, while WO_3 powders were placed at the center of high temperature furnace (furnace 2), in an inner quartz tube with a smaller diameter of 1 cm. The 2 cm by 2 cm substrate was then placed downstream in furnace 2, about 8.5 cm away from WO_3 powder. Figure 1(b) presents the temperature profiles employed for the formation of WS_2 on the SiO_2/Si substrate with four steps, including ramping, growth, sulfur purging and fast cooling. The whole system was first flushed with argon gas for 30 minutes, followed by a pre-introduction of S by heating the S powder up to 180 °C, which build an S-rich environment both before and during the synthesis of WS_2 monolayers. The second furnace was then heated up to 1150 °C with a ramping rate of 40 °C/min. The reaction was conducted once the temperature reached 1150 °C for a short period of time with a mixed gas flow. After purging the abundant sulfur away from the system, a fast cooling process was then applied when furnace 2 reached 850 °C. By optimizing the reaction parameters, such as the growth time, the growth temperature, the amounts of the precursors, the position of the substrate and hydrogen to argon (H_2/Ar) ratio, we can produce either monocrystalline monolayer WS_2 domains or large-area continuous polycrystalline monolayer WS_2 films for different purposes. Figures 1(d) and (c) are the photos of monolayer WS_2 samples after growth with and without H_2 addition, respectively. Figure 1(e) presents the SEM image of the blue rectangular dashed area in Figure 1(c), showing that large triangular WS_2 crystals with domain size of over 150 μm can be deposited on SiO_2/Si substrate with optimized growth variables without the addition of H_2 . As can be seen from Figure 1(f), the SEM image of the black rectangular dashed region in Figure 1(d), centimeter-sized continuous WS_2 films can be formed when the appropriate H_2/Ar ratio was used.

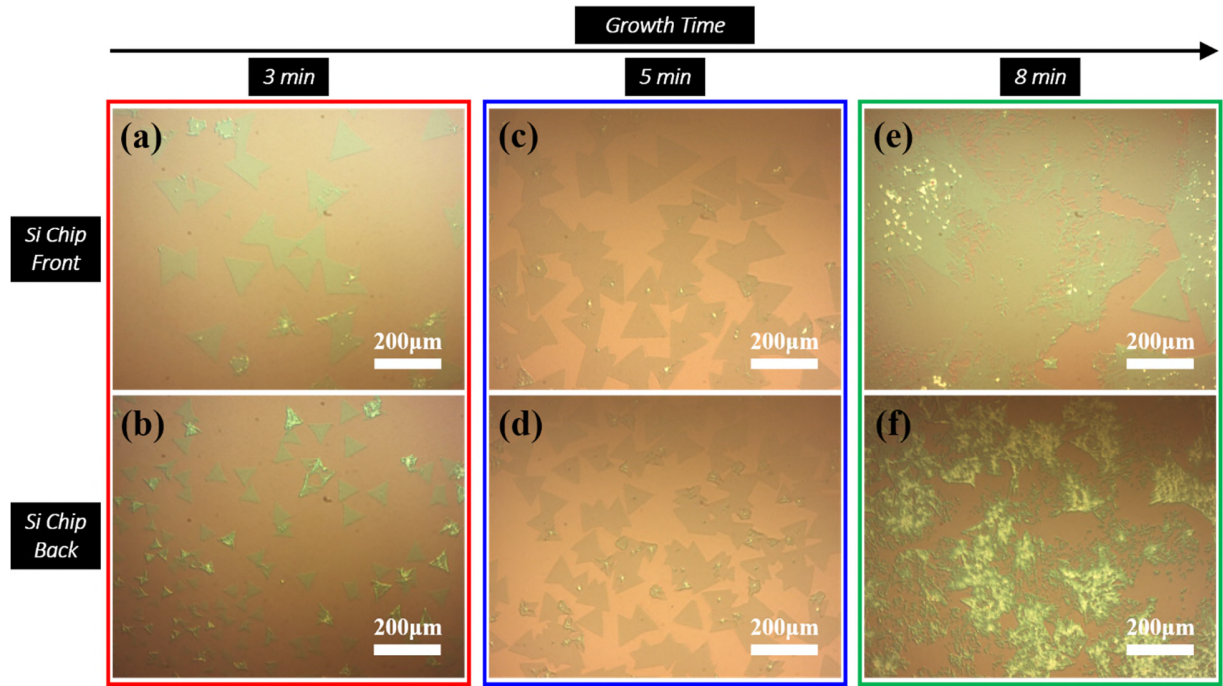


Figure 2. Optical images showing the CVD growth results as a function of growth time, when no hydrogen is used. (a-f) Optical images of the WS₂ on both the front and back side of the SiO₂/Si substrate after growth times of 3, 5 and 8 minutes, respectively. Scale bar: 200 μm . The substrate used for 5 minutes growth has an oxide layer of 90 nm thickness, while the other two have 300 nm oxide layers, causing the difference in contrast.

In order to explore continuous WS₂ films growth by APCVD, we first investigated whether it would be viable to simply extending the growth time for the previously reported synthesis procedure we developed for large monolayer domain growth of WS₂.³⁷ Figure 2 shows the optical images of the samples on both the front and the back regions of the SiO₂/Si substrates produced using different growth times (3, 5 and 8 minutes). For each growth time, the WS₂ domain size on the front side of the substrate is slightly larger than that on the back, and the back region is more likely to form multilayer WS₂ flakes. If grown for 3 minutes, Figures 2(a) and (b), the typical domain size is about 100 μm on the front region of the substrate and around 50 μm on the back

region. When the growth time is increased to 5 minutes, higher surface coverage was obtained, Figures 2(c) and (d), with larger domain size and higher nucleation density. However, increasing the growth time to 8 minutes led to multi-layer WS₂ crystals instead of a fully continuous monolayer film, Figures 2(e) and (f).

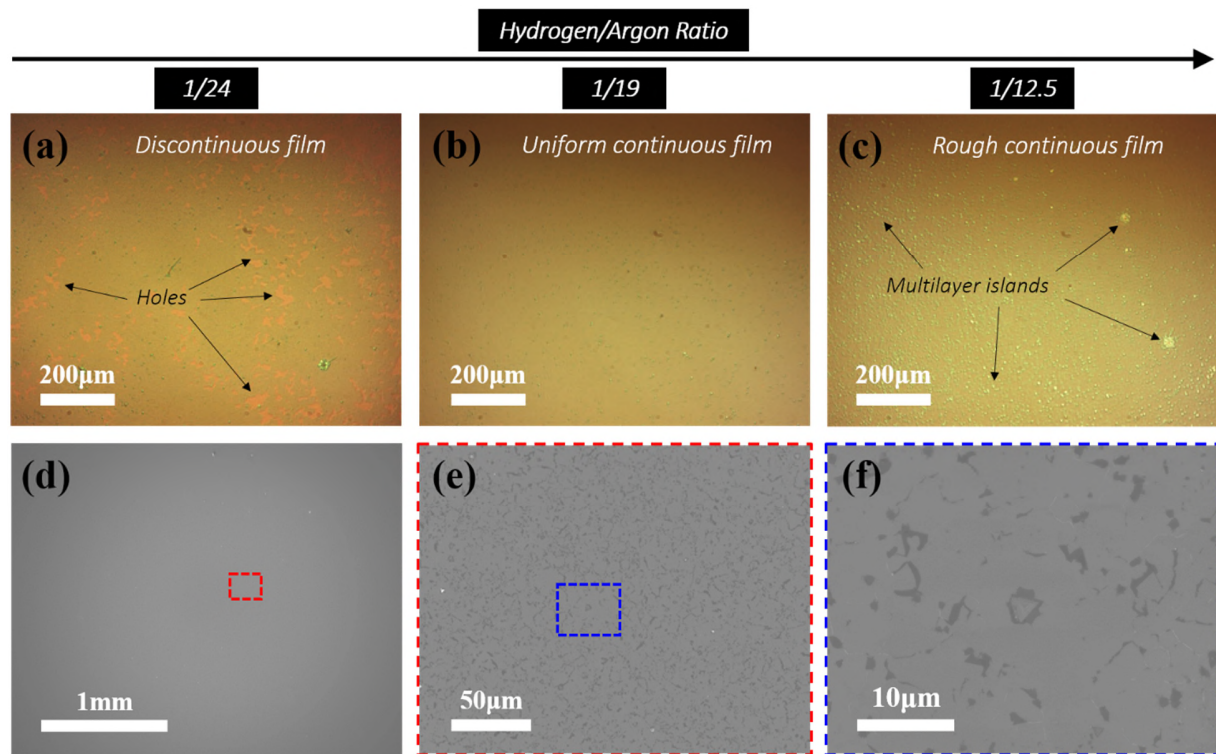


Figure 3. Surface morphology of WS₂ films with different H₂/Ar flow rate during the 3-minute growth.

(a-c) Optical images showing the result of growths using different H₂/Ar ratios, showing a semi-continuous film, a uniform continuous film and a rough continuous film, respectively. Scale bar: 200 μm. (d) SEM images of an as-grown WS₂ film with a H₂/Ar ratio of 1/19 during growth. Scale bar: 1 mm. (e, f) Zoomed-in SEM images chosen from the selected area, red dashed region in (d) and blue dashed region in (e) respectively, showing a continuous film with small multilayer islands. Scale bar represents 50 μm in (e) and 10 μm in (f).

Figure 3 shows the impact adding H₂ has on the APCVD growth of WS₂. The role of H₂ during the reaction is to increase the reaction speed and reduce damage from oxidization. The growth time was set to 3 minutes for all growths involving H₂. Figures 3(a-c) show the change in morphology of WS₂ films produced using different H₂/Ar ratios (1/24, 1/19, 1/12.5). A semi-continuous WS₂ film with holes, Figure 3(a), can be produced with less H₂ added, while a rougher continuous film

with several multilayer islands (Figure 3(c)) is fabricated when increasing the flow of H_2 during the growth. The optimized H_2/Ar ratio ($\sim 1/19$) was between these values, leading to fully continuous WS_2 films of high uniformity, Figure 3(b). Figure 3(d) presents the SEM image of a typical region of the sample grown with a H_2/Ar ratio of 1/19, indicating full coverage and high uniformity. Figures 3(e) and (f) show the magnified high-resolution SEM images of the red dashed rectangle in Figure 3(d) and the blue dashed rectangle in Figure 3(e) respectively, the WS_2 film is highly uniform over the whole area under SEM observation with up to 95% monolayer and only a small amount of multilayer regions.

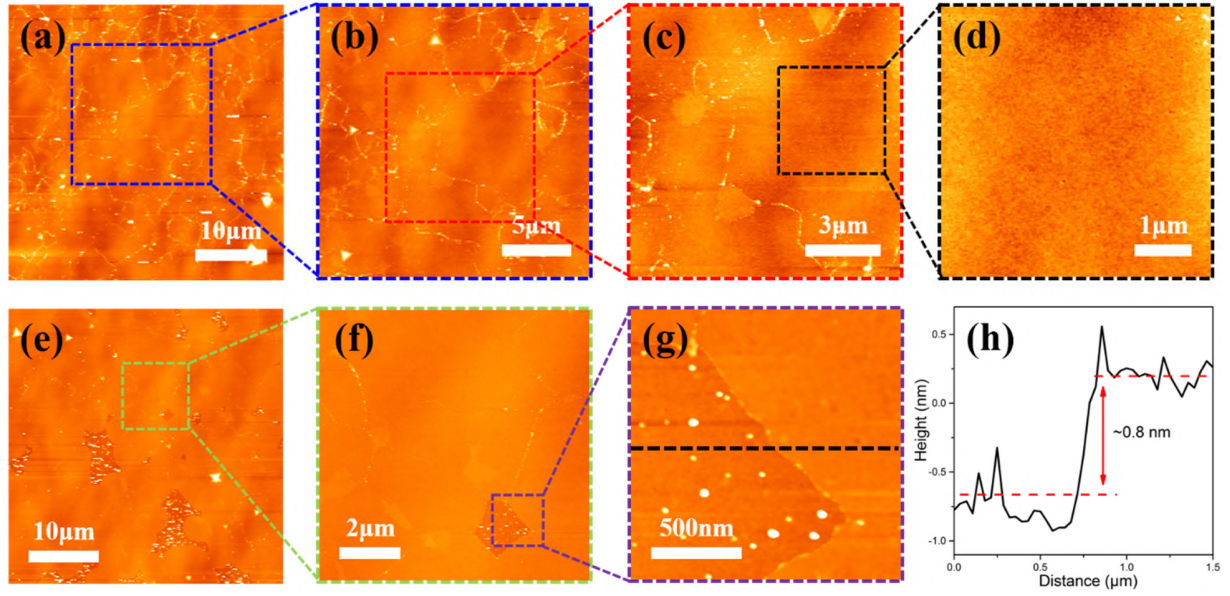


Figure 4. AFM measurement of as-grown WS₂ films on SiO₂/Si. (a-d) AFM image in topological mode of a fully-merged WS₂ region and zoomed-in images chosen from the selected area, showing very uniform surface. Scale bar represents 10 μm in (a), 5 μm in (b), 3 μm in (c), and 1 μm in (d). (e-g) AFM image of a typical growth region near the edge of substrate and zoomed-in images obtained from the same area, showing some holes and wrinkles. Scale bar represents 10 μm in (e), 2 μm in (f) and 500 nm in (g). (h) Height profile taken from the black dashed line in (g), showing that the thickness of WS₂ film is about 0.8 nm.

The roughness and thickness of the fabricated continuous WS₂ films were characterized by AFM. Figure 4(a) shows the surface morphology of a typical continuous region and Figures 4(b) and (c) are the zoomed-in images chosen from the selected areas, showing grain boundaries and some nucleation sites on the surface. The further zoomed-in image, Figure 4(d), shows a uniform monolayer thickness and small surface roughness of ~0.2 nm. At the edge of the sample, some discontinuous regions can be found. Figures 4(e-g) show AFM image of a typical area near the edge and the zoomed-in images obtained from the corresponding regions. Besides grain boundaries and nucleation sites, some holes in the WS₂ film. Figure 4(h) presents the height profile of the

black dashed line in Figure 4(g), which shows that the height difference between the film and the substrate is about 0.8 nm, confirming monolayer WS₂.⁴⁰

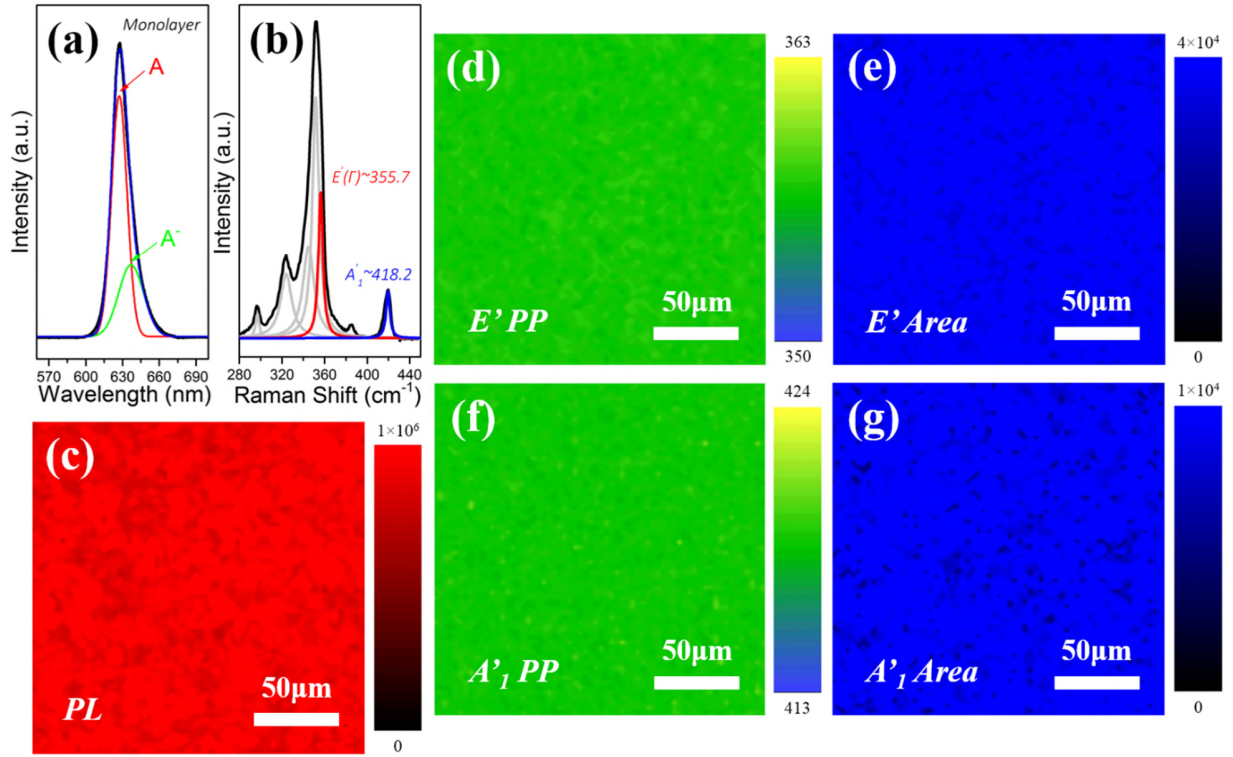


Figure 5. Raman and PL measurements of as-grown WS₂ films on SiO₂/Si. (a) PL and (b) Raman spectrum of the as-grown sample, confirming monolayer WS₂. (c-g) PL and Raman maps of a typical area (200 μm by 200 μm) of the WS₂ continuous film, showing (c) PL integrated intensity, (d) E' peak position and (e) integrated intensity as well as (f) A₁' peak position and (g) integrated intensity, indicating high uniformity. Scale bar: 50 μm.

The as-grown continuous WS₂ film was further investigated using PL and Raman spectroscopy with a 532 nm excitation to determine the layer number and quality. Figure 5(a) shows a strong PL peak between 560 nm to 700 nm, typical for a CVD grown monolayer WS₂ sample. The PL signal was then deconvoluted into two separate peaks by fitting Gaussian curves, which correspond to the exciton emission (A) and negative trion emission (A⁻). The peak position for A is 627.3 nm, a direct band gap of ~1.98 eV, which falls in the range of reported PL peak positions for monolayer WS₂ samples with strain from the CVD cooling process.^{27,39} The peak position for A⁻ is 636.9 nm,

leading to a binding energy of ~ 30 meV for our continuous WS₂ film, which is also in agreement with the values ranging from 20 to 40 meV reported previously.^{41,42} The integrated PL intensity ratio of exciton to trion (A/A^-) was used to determine the doping level of the WS₂, and was measured to be 2.1, indicative of high quality material. Raman spectroscopy was also used to examine the quality of the WS₂ film. A Raman spectrum taken from a typical spot on our continuous monolayer WS₂ film was fitted by multiple Lorentzian peaks, Figure 5(b), with the peak positions for in-plane (E') and out-of-plane (A'_1) vibration modes at 355.7 and 418.2 cm⁻¹ respectively. The frequency difference between E' and A'_1 mode is shown to be ~ 62.5 cm⁻¹, which is in agreement with our previous reports.^{29,43-46} PL and Raman mappings were carried out to evaluate the areal uniformity, Figures 5(c-g). Figure 5(c) presents the PL integrated intensity mapping of a typical region of the sample with area of 200 μm by 200 μm , indicating a high uniformity of the monolayer WS₂ film. Figures 5(d-g) show the Raman mappings obtained from the same region as the PL mapping, including peak position and integrated intensity of the WS₂ E' and A'_1 modes. After fitted with Lorentzian curves, Raman spectra ranging between 280 to 440 cm⁻¹ can be deconvoluted into six separate peaks, two of which correspond to WS₂ E' and A'_1 modes. As shown in Figures 5(d) and (f), the average peak positions for E' and A'_1 modes are 357.0 and 418.7 cm⁻¹ respectively, indicating high quality and uniformity of the film produced. Figures 5(e) and (g) show the Raman maps for the integrated intensity of E' and A'_1 modes respectively, also confirming a homogeneous monolayer.

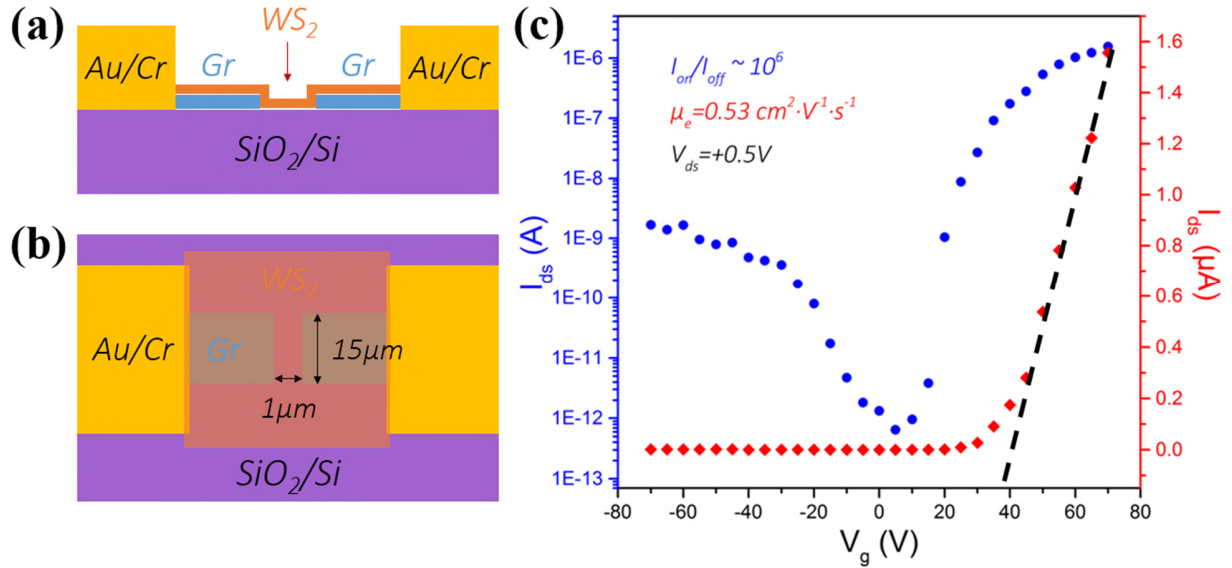


Figure 6. Electrical properties of monolayer WS_2 continuous film. (a) Schematic side view of a FET based on monolayer WS_2 continuous film with graphene electrodes. (b) Schematic top view of the WS_2 FET with a channel length of $1\mu\text{m}$ and a channel width of $15\mu\text{m}$. (c) The field effect characteristics of the as-grown monolayer WS_2 FET. I_{ds} - V_g (red curve) shows the N-type characteristics of the device with a threshold voltage V_{th} of $\sim 35\text{V}$. The ON/OFF ratio of output current (blue curve) is $\sim 10^6$ at room temperature.

To evaluate the electrical properties of our monolayer WS_2 continuous film, field effect transistors were fabricated by the transfer of WS_2 film onto the 300 nm SiO_2/Si substrate prepatterned with graphene electrodes. Figures 6(a) and (b) illustrate the side and top views of the FET based on our monolayer WS_2 continuous film, showing a channel length of $1\mu\text{m}$ and a channel width of $15\mu\text{m}$. The electrical properties of the WS_2 FET were measured in air under ambient pressure within a $\pm 70\text{V}$ gate bias, which was applied through a heavily p-doped silicon underneath the 300 nm SiO_2 dielectric. A typical gate sweep measurement, red curve in Figure 6(c), shows a well-defined N-typed transistor with a threshold voltage (V_{th}) of $\sim 35\text{ V}$. We extracted the field-effect electron mobility (μ_{FE}) using the following expression:

$$\mu_{FE} = \frac{dI_{ds}}{dV_g} \cdot \frac{L}{w} \cdot \frac{1}{V_{ds}} \cdot \frac{1}{C_{ox}}$$

where $\frac{dI_{ds}}{dV_g}$ is the transconductance, L is the channel length, w is the channel width, V_{ds} is the applied drain bias and C_{ox} is the gate capacitance.^{40,47} Our WS₂ FET shows a FET mobility of 0.53 cm² V⁻¹ s⁻¹ at room temperature, which is amongst the best reported for CVD-grown polycrystalline WS₂ monolayers measured using similar back gated doped Si electrodes on SiO₂ surfaces.^{48,49} In addition, at an applied drain bias of 0.5 V, an on/off ratio of $\sim 10^6$ and an subthreshold swing of 2.05 V per decade were obtained, which is also in agreement with the previous works.⁴⁹⁻⁵⁴

Figures 1-5 indicate that the introduction of H₂ to our double-furnace system produces substantially different growth morphologies compared to the isolated WS₂ flakes synthesized using the same experimental conditions but without H₂. Without H₂ addition, multi-layer WS₂ islands form before a fully-merged continuous monolayer film is complete. The addition of H₂ during synthesis may reduce the WO₃ precursor more effectively, leading to a higher nucleation density and fast completion of the continuous films before secondary layers begin to form.^{33,56} It is worth mentioning that the growth with H₂ usually results in a smaller domain size than that without H₂, resulting in an increased number of grain boundaries on the surface. This is similar to a prior report, where domain size decreased with hydrogen.⁵⁵ The electrical properties of the FET devices based on the continuous films, Figure 6, is slightly better than that using our isolated WS₂ domains.⁵⁰ This indicates that H₂ addition may also aid in removing carbonaceous species and reducing the amount of WS₂ oxidation during growth, and therefore lead to better quality WS₂.^{32,55}

CONCLUSION

In summary, we present a scalable, rapid, and bottom-up approach for growing large-area monolayer WS₂ continuous films using APCVD. Without introducing H₂ to the double-furnace system, we are able to grow separately distributed WS₂ flakes on SiO₂/Si with domain sizes of at least 150 μm when the growth time was increased from 3 to 5 minutes. Further increasing the growth time to 8 minutes led to vertical growth, forming multilayers instead of a fully-merged monolayer film. The introduction of H₂ allows the rapid formation of WS₂ continuous films before the emergence of multilayer islands. With an optimized H₂/Ar ratio and short growth time (3 minutes), centimeter-scale continuous WS₂ films can be directly grown on silicon wafers with an oxide surface, indicating high efficiency of our APCVD system. The results from optical microscopy, SEM, AFM, PL spectroscopy, Raman spectroscopy and FETs have confirmed its high quality and uniformity. This rapid APCVD growth method utilizing simple and frequently-used powder precursors will facilitate the further development of wafer scale optoelectronic devices based on all CVD-grown 2D materials.

EXPERIMENTAL METHODS

CVD Synthesis of Monolayer WS₂ continuous film

The CVD monolayer WS₂ films were fabricated on SiO₂/Si substrates (University Wafer) based on our previously reported CVD approach³⁷⁻³⁹ using S and WO₃ as precursors, but with the addition of H₂. Before growth, the substrate was cleaned using sonication in acetone and isopropanol (IPA) for 15 minutes each, followed by a 10-minute oxygen plasma treatment. 200mg sulfur powder (>99.5%, Sigma-Aldrich) was loaded at the center of furnace 1 in the outer 1 inch quartz tube, while 100mg of WO₃ powder (>99.5%, Sigma-Aldrich) was placed at the center of furnace 2, in

an inner quartz tube with a smaller diameter of 1cm. The 2cm by 2cm substrate was then placed downstream in furnace 2, about 8.5cm away from WO_3 powder. The whole system was first flushed with 500 standard cubic centimeters per minute (sccm) argon gas (Ar) for 30 minutes, followed by a pre-introduction of S by heating the S powder up to 180 °C. Then furnace 2 was heated up to 1150 °C with a ramping rate of 40 °C/min. The reaction was conducted under the temperature of 1150 °C for 3 minutes with a mixed gas flow of 250 sccm and a H_2/Ar ratio of 1/19. After that, furnace 2 was set down to room temperature with an Ar flow of 10 sccm, whilst furnace 1 was heated up to 400 °C. The flow rate was set back to 500 sccm when furnace 2 reached 950 °C in order to purge the abundant S away from the system. A fast cooling process was then applied when furnace 2 reached 850 °C.

CVD Synthesis of graphene

A piece of 25 μm thick 99.8% copper (Goodfellow) was first sonicated in diluted hydrochloric acid solution (1 M), acetone and IPA for 2, 5 and 5 minutes, respectively. The CVD growth was then performed at atmospheric pressure and the receipt was based on our previous report.⁵ It was first purged with 2000 sccm Ar, 1000 sccm H_2 and 50 sccm methane (CH_4) for 30 minutes. The temperature of the furnace was set to 1060 °C at a ramping rate of 50 °C/min under a flow of 500 sccm of Ar and 100 sccm of H_2 . The copper was annealed at 1060 °C with the same flow rate for 1 hour. Graphene growth was carried out at 1060 °C under a flow of 500 sccm of Ar, 100 sccm of H_2 and 5 sccm of CH_4 for 1 hour. After growth, the furnace was slid away from the sample to the other end of the runners, which allows the sample to be fast cooled to room temperature.

Transfer of CVD-grown graphene and Monolayer WS_2 continuous film

The as-grown CVD samples were first spin-coated with a poly(methyl methacrylate) (PMMA) scaffold (8 wt % in anisole, 495k molecular weight) at 4500 rpm for 60 seconds and cured at 180 °C for 90 seconds. The PMMA/graphene film was separated from Cu substrate by ammonium persulfate (0.1 M) etching, while the PMMA/WS₂ film was separated from the growth substrate by potassium hydroxide (1 M) etching at 60 °C. The floating PMMA/graphene and PMMA/WS₂ films were carefully transferred several times into deionized water to dilute residual contaminations. The films were subsequently transferred onto other substrates and baked at 150 °C for 30 minutes for sample adhesion.

Device Fabrication

JEOL 5500 FS electron-beam lithography (EBL) system was used to pattern bond pads in a bilayer PMMA resist. A thermal evaporator was used to deposit Au/Cr (80 nm/10 nm) bond pads onto a 300 nm SiO₂/Si substrate, followed by liftoff in acetone at 45 °C. The PMMA/Graphene film was transferred onto the Si chip with prepatterned bond pads, and baked overnight at 180 °C for better contact. Graphene film was then patterned using EBL with negative resist and oxygen plasma etching to define graphene channels with a length and width of 1 and 15 μm respectively. Lastly, the PMMA/WS₂ film was transferred onto the sample. After baked at 150 °C for 30 minutes, the sample was rinsed in hot acetone for PMMA removal. The electrical measurements of the WS₂ FETs were carried out using a source meter (Keithley 2400 V). All the measurements were conducted in room-temperature under ambient pressure.

Characterization of Monolayer WS₂ continuous film

The morphology of the WS₂ continuous films on SiO₂/Si were characterized using a scanning electron microscope (Hitachi S-4300) with an accelerating voltage of 3.0 kV. Raman spectroscopy

and photoluminescence was carried out using a JY Horiba LabRAM Aramis imaging confocal Raman microscope with an excitation wavelength of 532 nm with an estimated laser spot size of 1 μ m. The laser power was 125 μ W for PL measurement and 12.5 mW for Raman spectroscopy. Thickness characterizations of as-grown WS₂ films were performed using an atomic force microscope (Asylum Research MFP-3D) in AC mode with a silicon AC-160TS cantilever (Olympus, spring constant \sim 42 N/m and resonant frequency \sim 300 kHz).

AUTHOR INFORMATION

Corresponding Author

*Email: jamie.warner@materials.ox.ac.uk.

Notes

The authors declare no competing financial interest.

ACKNOWLEDGEMENTS

J.H.W. thanks the Royal Society for support. Y.S. acknowledges support from Great Britain-China Educational Trust and St Cross College, Oxford.

REFERENCES

- (1) Wang, Q. H.; Kalantar-Zadeh, K.; Kis, A.; Coleman, J. N.; Strano, M. S. Electronics and Optoelectronics of Two-Dimensional Transition Metal Dichalcogenides. *Nat. Nanotechnol.* **2012**, *7*, 699–712.
- (2) Geim, A. K.; Novoselov, K. S. The Rise of Graphene. *Nat. Mater.* **2007**, *6*, 183–191.
- (3) Li, X.; Cai, W.; An, J.; Kim, S.; Nah, J.; Yang, D.; Piner, R.; Velamakanni, A.; Jung, I.; Tutuc, E.; et al. Large-Area Synthesis of High-Quality and Uniform Graphene Films on Copper Foils. *Science* **2009**, *324*, 1312–1314.
- (4) Bae, S.; Kim, H.; Lee, Y.; Xu, X.; Park, J.-S.; Zheng, Y.; Balakrishnan, J.; Lei, T.; Kim, H. R.; Song, Y. I.; et al. Roll-to-Roll Production of 30-Inch Graphene Films for Transparent Electrodes. *Nat. Nanotechnol.* **2010**, *5*, 574–578.
- (5) Sheng, Y.; Rong, Y.; He, Z.; Fan, Y.; Warner, J. H. Uniformity of Large-Area Bilayer Graphene Grown by Chemical Vapor Deposition. *Nanotechnology* **2015**, *26*, 395601.
- (6) Hwang, J. O.; Park, J. S.; Choi, D. S.; Kim, J. Y.; Lee, S. H.; Lee, K. E.; Kim, Y. H.; Song, M. H.; Yoo, S.; Kim, S. O. Workfunction-Tunable, N-Doped Reduced Graphene Transparent Electrodes for High-Performance Polymer Light-Emitting Diodes. *ACS Nano* **2012**, *6*, 159–167.
- (7) Shim, J.; Yun, J. M.; Yun, T.; Kim, P.; Lee, K. E.; Lee, W. J.; Ryoo, R.; Pine, D. J.; Yi, G. R.; Kim, S. O. Two-Minute Assembly of Pristine Large-Area Graphene Based Films. *Nano Lett.* **2014**, *14*, 1388–1393.

- (8) Ci, L.; Song, L.; Jin, C.; Jariwala, D.; Wu, D.; Li, Y.; Srivastava, A.; Wang, Z. F.; Storr, K.; Balicas, L.; et al. Atomic Layers of Hybridized Boron Nitride and Graphene Domains. *Nat. Mater.* **2010**, *9*, 430–435.
- (9) Dean, C. R.; Young, A. F.; Meric, I.; Lee, C.; Wang, L.; Sorgenfrei, S.; Watanabe, K.; Taniguchi, T.; Kim, P.; Shepard, K. L.; et al. Boron Nitride Substrates for High-Quality Graphene Electronics. *Nat. Nanotechnol.* **2010**, *5*, 722–726.
- (10) Liu, Z.; Song, L.; Zhao, S.; Huang, J.; Ma, L.; Zhang, J.; Lou, J.; Ajayan, P. M. Direct Growth of Graphene/hexagonal Boron Nitride Stacked Layers. *Nano Lett.* **2011**, *11*, 2032–2037.
- (11) Wang, X.; Hooper, T. N.; Kumar, A.; Priest, I. K.; Sheng, Y.; Samuels, T. O. M.; Wang, S.; Robertson, A. W.; Pacios, M.; Bhaskaran, H.; et al. Oligomeric Aminoborane Precursors for the Chemical Vapour Deposition Growth of Few-Layer Hexagonal Boron Nitride. *CrystEngComm* **2016**, *19*, 285–294.
- (12) Yun, S. J.; Chae, S. H.; Kim, H.; Park, J. C.; Park, J. H.; Han, G. H.; Lee, J. S.; Kim, S. M.; Oh, H. M.; Seok, J.; et al. Synthesis of Centimeter-Scale Monolayer Tungsten Disulfide Film on Gold Foils. *ACS Nano* **2015**, *9*, 5510–5519.
- (13) Loh, T. A. J.; Chua, D. H. C.; Wee, A. T. S. One-Step Synthesis of Few-Layer WS₂ by Pulsed Laser Deposition. *Sci. Rep.* **2015**, *5*, 18116.
- (14) Loan, P. T. K.; Zhang, W.; Lin, C.-T.; Wei, K.-H.; Li, L.-J.; Chen, C.-H. Graphene/MoS₂ Heterostructures for Ultrasensitive Detection of DNA Hybridisation. *Adv. Mater.* **2014**, *26*, 4838–4844.

- (15) Lopez-Sanchez, O.; Lembke, D.; Kayci, M.; Radenovic, A.; Kis, A. Ultrasensitive Photodetectors Based on Monolayer MoS₂. *Nat. Nanotechnol.* **2013**, *8*, 497–501.
- (16) Lopez-Sanchez, O.; Alarcon Llado, E.; Koman, V.; Fontcuberta I Morral, A.; Radenovic, A.; Kis, A. Light Generation and Harvesting in a van Der Waals Heterostructure. *ACS Nano* **2014**, *8*, 3042–3048.
- (17) Bernardi, M.; Palummo, M.; Grossman, J. C. Extraordinary Sunlight Absorption and One Nanometer Thick Photovoltaics Using Two-Dimensional Monolayer Materials. *Nano Lett.* **2013**, *13*, 3664–3670.
- (18) Yin, W.; Yan, L.; Yu, J.; Tian, G.; Zhou, L.; Zheng, X.; Zhang, X.; Yong, Y.; Li, J.; Gu, Z.; et al. High-Throughput Synthesis of Single-Layer MoS₂ Nanosheets as a near-Infrared Photothermal-Triggered Drug Delivery for Effective Cancer Therapy. *ACS Nano* **2014**, *8*, 6922–6933.
- (19) Mao, D.; Wang, Y.; Ma, C.; Han, L.; Jiang, B.; Gan, X.; Hua, S.; Zhang, W.; Mei, T.; Zhao, J. WS₂ Mode-Locked Ultrafast Fiber Laser. *Sci. Rep.* **2015**, *5*, 7965.
- (20) Hamm, J. M.; Hess, O. Two Two-Dimensional Materials Are Better than One. *Science* **2013**, *340*, 1298–1299.
- (21) Eda, G.; Maier, S. A. Two-Dimensional Crystals: Managing Light for Optoelectronics. *ACS Nano*, **2013**, *7*, 5660–5665.
- (22) Geim, A. K.; Grigorieva, I. V. Van Der Waals Heterostructures. *Nature* **2013**, *499*, 419–425.

- (23) Novoselov, K. S.; Jiang, D.; Schedin, F.; Booth, T. J.; Khotkevich, V. V.; Morozov, S. V.; Geim, A. K. Two-Dimensional Atomic Crystals. *Proc. Natl. Acad. Sci. U. S. A.* **2005**, *102*, 10451–10453.
- (24) Yun, T.; Kim, J.-S.; Shim, J.; Choi, D. S.; Lee, K. E.; Koo, S.; Kim, I.; Jung, H. J.; Yoo, H.-W.; Jung, H.-T.; *et al.* Ultrafast Interfacial Self-Assembly of 2D Transition Metal Dichalcogenides Monolayer Films and Their Vertical and In-Plane Heterostructures. *ACS Appl. Mater. Interfaces* **2017**, *9*, 1021–1028.
- (25) Zhao, W.; Ghorannevis, Z.; Chu, L.; Toh, M.; Kloc, C.; Tan, P.-H.; Eda, G. Evolution of Electronic Structure in Atomically Thin Sheets of WS₂ and WSe₂. *ACS Nano* **2013**, *7*, 791–797.
- (26) Zeng, Z.; Yin, Z.; Huang, X.; Li, H.; He, Q.; Lu, G.; Boey, F.; Zhang, H. Single-Layer Semiconducting Nanosheets: High-Yield Preparation and Device Fabrication. *Angew. Chem. Int. Ed.* **2011**, *50*, 11093–11097.
- (27) Zeng, H.; Liu, G.-B.; Dai, J.; Yan, Y.; Zhu, B.; He, R.; Xie, L.; Xu, S.; Chen, X.; Yao, W.; *et al.* Optical Signature of Symmetry Variations and Spin-Valley Coupling in Atomically Thin Tungsten Dichalcogenides. *Sci. Rep.* **2013**, *3*, 1608.
- (28) Coleman, J. N.; Lotya, M.; O'Neill, A.; Bergin, S. D.; King, P. J.; Khan, U.; Young, K.; Gaucher, A.; De, S.; Smith, R. J.; *et al.* Two-Dimensional Nanosheets Produced by Liquid Exfoliation of Layered Materials. *Science* **2011**, *331*, 568–571.
- (29) Gutiérrez, H. R.; Perea-López, N.; Elías, A. L.; Berkdemir, A.; Wang, B.; Lv, R.; López-Urías, F.; Crespi, V. H.; Terrones, H.; Terrones, M. Extraordinary Room-Temperature Photoluminescence in Triangular WS₂ Monolayers. *Nano Lett.* **2013**, *13*, 3447–3454.

- (30) Elías, A. L.; Perea-López, N.; Castro-Beltrán, A.; Berkdemir, A.; Lv, R.; Feng, S.; Long, A. D.; Hayashi, T.; Kim, Y. A.; Endo, M.; et al. Controlled Synthesis and Transfer of Large-Area WS₂ Sheets : From Single Layer to Few Layers. *ACS Nano* **2013**, *7*, 5235–5242.
- (31) Hussain, S.; Khan, M. F.; Shehzad, M. A.; Vikraman, D.; Iqbal, M. Z.; Choi, D.-C.; Song, W.; An, K.-S.; Seo, Y.; Eom, J.; et al. Layer-Modulated, Wafer Scale and Continuous Ultra-Thin WS₂ Films Grown by RF Sputtering: Via Post-Deposition Annealing. *J. Mater. Chem. C* **2016**, *4*, 7846–7852.
- (32) Kang, K. N.; Godin, K.; Yang, E. H. The Growth Scale and Kinetics of WS₂ Monolayers under Varying H₂ Concentration. *Sci. Rep.* **2015**, *5*, 13205.
- (33) McCreary, K. M.; Hanbicki, A. T.; Jernigan, G. G.; Culbertson, J. C.; Jonker, B. T. Synthesis of Large-Area WS₂ Monolayers with Exceptional Photoluminescence. *Sci. Rep.* **2016**, *6*, 19159.
- (34) Perea-López, N.; Elías, A. L.; Berkdemir, A.; Castro-Beltrán, A.; Gutiérrez, H. R.; Feng, S.; Lv, R.; Hayashi, T.; López-Urías, F.; Ghosh, S.; et al. Photosensor Device Based on Few-Layered WS₂ Films. *Adv. Funct. Mater.* **2013**, *23*, 5511–5517.
- (35) Lee, Y. H.; Yu, L.; Wang, H.; Fang, W.; Ling, X.; Shi, Y.; Lin, C. Te; Huang, J. K.; Chang, M. T.; Chang, C. S.; et al. Synthesis and Transfer of Single-Layer Transition Metal Disulfides on Diverse Surfaces. *Nano Lett.* **2013**, *13*, 1852–1857.
- (36) Gao, Y.; Liu, Z.; Sun, D.-M.; Huang, L.; Ma, L.-P.; Yin, L.-C.; Ma, T.; Zhang, Z.; Ma, X.-L.; Peng, L.-M.; et al. Large-Area Synthesis of High-Quality and Uniform Monolayer WS₂ on Reusable Au Foils. *Nat. Commun.* **2015**, *6*, 8569.

- (37) Rong, Y.; Fan, Y.; Leen Koh, A.; Robertson, A. W.; He, K.; Wang, S.; Tan, H.; Sinclair, R.; Warner, J. H. Controlling Sulphur Precursor Addition for Large Single Crystal Domains of WS₂. *Nanoscale* **2014**, *6*, 12096–12103.
- (38) Rong, Y.; He, K.; Pacios, M.; Robertson, A. W.; Bhaskaran, H.; Warner, J. H. Controlled Preferential Oxidation of Grain Boundaries in Monolayer Tungsten Disulfide for Direct Optical Imaging. *ACS Nano* **2015**, *9*, 3695–3703.
- (39) Rong, Y.; Sheng, Y.; Pacios, M.; Wang, X.; He, Z.; Bhaskaran, H.; Warner, J. H. Electroluminescence Dynamics across Grain Boundary Regions of Monolayer Tungsten Disulfide. *ACS Nano* **2016**, *10*, 1093–1100.
- (40) Iqbal, M. W.; Iqbal, M. Z.; Khan, M. F.; Shehzad, M. A.; Seo, Y.; Park, J. H.; Hwang, C.; Eom, J. High-Mobility and Air-Stable Single-Layer WS₂ Field-Effect Transistors Sandwiched between Chemical Vapor Deposition-Grown Hexagonal BN Films. *Sci. Rep.* **2015**, *5*, 9.
- (41) Zhu, B.; Chen, X.; Cui, X. Exciton Binding Energy of Monolayer WS₂. *Sci. Rep.* **2014**, *5*, 9218.
- (42) Plechinger, G.; Nagler, P.; Kraus, J.; Paradiso, N.; Strunk, C.; Schüller, C.; Korn, T. Identification of Excitons, Trions and Biexcitons in Single-Layer WS₂. *Phys. Status Solidi - Rapid Res. Lett.* **2015**, *9*, 457–461.
- (43) He, Z.; Xu, W.; Zhou, Y.; Wang, X.; Sheng, Y.; Rong, Y.; Guo, S.; Zhang, J.; Smith, J. M.; Warner, J. H. Biexciton Formation in Bilayer Tungsten Disulfide. *ACS Nano* **2016**, *10*, 2176–2183.

- (44) He, Z.; Sheng, Y.; Rong, Y.; Lee, G.; Li, J.; Warner, J. H. Layer-Dependent Modulation of Tungsten Disulfide Photoluminescence by Lateral Electric Fields. *ACS Nano* **2015**, *9*, 2740–2748.
- (45) Sheng, Y.; Xu, W.; Wang, X.; He, Z.; Rong, Y.; Warner, J. H. Mixed Multilayered Vertical Heterostructures Utilizing Strained Monolayer WS₂. *Nanoscale* **2016**, *8*, 2639–2647.
- (46) Sheng, Y.; Wang, X.; Fujisawa, K.; Ying, S.; Elias, A. L.; Lin, Z.; Xu, W.; Zhou, Y.; Korsunsky, A. M.; Bhaskaran, H.; Terrones, M.; Warner, J. H. Photoluminescence Segmentation within Individual Hexagonal Monolayer Tungsten Disulfide Domains Grown by Chemical Vapor Deposition. *ACS Appl. Mater. Interfaces*, **2017**, *9*, 15005–15014.
- (47) Zhan, Y.; Liu, Z.; Najmaei, S.; Ajayan, P. M.; Lou, J. Large-Area Vapor-Phase Growth and Characterization of MoS₂ Atomic Layers on a SiO₂ Substrate. *Small* **2012**, *8*, 966–971.
- (48) Orofeo, C. M.; Suzuki, S.; Sekine, Y.; Hibino, H. Scalable Synthesis of Layer-Controlled WS₂ and MoS₂ Sheets by Sulfurization of Thin Metal Films. *Appl. Phys. Lett.* **2014**, *105*.
- (49) Lan, C.; Li, C.; Yin, Y.; Liu, Y. Large-Area Synthesis of Monolayer WS₂ and Its Ambient-Sensitive Photo-Detecting Performance. *Nanoscale* **2015**, *7*, 5974–5980.
- (50) Tan, H.; Fan, Y.; Zhou, Y.; Chen, Q.; Xu, W.; Warner, J. H. Ultrathin 2D Photodetectors Utilizing Chemical Vapor Deposition Grown WS₂ with Graphene Electrodes. *ACS Nano* **2016**, *10*, 7866–7873.
- (51) Fan, Y.; Zhou, Y.; Wang, X.; Tan, H.; Rong, Y.; Warner, J. H. Photoinduced Schottky Barrier Lowering in 2D Monolayer WS₂ Photodetectors. *Adv. Opt. Mater.* **2016**, *4*, 1573–1581.
- (52) Song, J. G.; Park, J.; Lee, W.; Choi, T.; Jung, H.; Lee, C. W.; Hwang, S. H.; Myoung, J. M.;

- Jung, J. H.; Kim, S. H.; *et al.* Layer-Controlled, Wafer-Scale, and Conformal Synthesis of Tungsten Disulfide Nanosheets Using Atomic Layer Deposition. *ACS Nano* **2013**, *7*, 11333–11340.
- (53) Ovchinnikov, D.; Allain, A.; Huang, Y.-S.; Dumcenco, D. Electrical Transport Properties of Single-Layer WS₂. *ACS Nano* **2014**, *8*, 8174–8181.
- (54) Iqbal, M. W.; Iqbal, M. Z.; Khan, M. F.; Kamran, M. A.; Majid, A.; Alharbi, T.; Eom, J. Tailoring the Electrical and Photo-Electrical Properties of a WS₂ Field Effect Transistor by Selective N-Type Chemical Doping. *RSC Adv.* **2016**, *6*, 24675–24682.
- (55) Kang, K.; Xie, S.; Huang, L.; Han, Y.; Huang, P. Y.; Mak, K. F.; Kim, C.-J.; Muller, D.; Park, J. High-Mobility Three-Atom-Thick Semiconducting Films with Wafer-Scale Homogeneity. *Nature* **2015**, *520*, 656–660.
- (56) Zhang, Y.; Zhang, Y.; Ji, Q.; Ju, J.; Yuan, H.; Shi, J.; Gao, T.; Ma, D.; Liu, M.; Chen, Y.; *et al.* Controlled Growth of High-Quality Monolayer WS₂ Layers on Sapphire. *ACS Nano* **2013**, *7*, 8963–8971.

TOC GRAPHIC

